Wire Arc Additive Manufacturing of Steel: Deposition Patterns Effect on Microstructure and Mechanical Properties

Arzaq Al-Roubaiy[1*], Saad Al-Shafaie [1] and Abdul Sameea Jilabi[1]
[1] Faculty of Materials Engineering/University of Babylon, Hilla, Babil, Iraq

Abstract. Recently, Metal Inert Gas (MIG) -based weld deposition process is one of the deposition-based Additive Manufacturing (AM) processes. This technique has created considerable interest due to the advantages it offers of being able to produce fully functional, complex, dense metallic objects. The study mainly aims to investigate the influence of a variety of deposition patterns on the microstructure and the mechanical properties of steel materials built on a low alloy steel substrate by MIG process. Experiments were carried out using a semi-automated MIG welding to built the samples manufactured using five different deposition patterns (longitudinal, transverse, right network, oblique and oblique network). Microscopy generally showed coarse equiaxed grains in the lower regions ،fine equiaxed grains in the middle regions and columnar grains in the upper regions. The maximum hardness was (201HV) for the sample built with the oblique pattern, while the minimum hardness was (170 HV) for the sample built longitudinally. The highest average tensile strength value was (480 MPa) for the sample built longitudinally. The fracture mode was significantly ductile.The lowest average tensile strength value was however (262.5 MPa) for the sample built transversely, and the fracture mode was brittle.

1 Introduction

The process of depositing weld metal to produce whole components has been employed since 1920, and it is today known as wire arc additive manufacturing (WAAM). This approach offers various advantages over traditional production methods, including a higher buy-to-fly (BTF) ratio, the flexibility to possibly ignore the size limit of component fabrication, and cost-effectiveness as compared to powder-based procedures that rely on expensive materials [1]. According to ASTM F2792-12a, WAAM is a wire-feed AM method that includes indirect energy deposition (DED) [2]. It is also known as an electric arc heat source and a raw material formed of metal wire. The concept of WAAM is based on the automatic welding process. WAAM has been referred to as rapid prototyping (RP), shape melting (SM) and shape welding (SW), shape metal deposition (SMD), solid freeform fabrication (SFF), and even 3D welding in recent years [3]. Depending on the nature of the heat source, there are three types of WAAM approaches (Figure 1) [2]: GMAW (Gas Metal Arc Welding), GTAW

* Corresponding author: qqqq58928@gmail.com

(Gas Tungsten Arc Welding) and PAW (Plasma Arc Welding).

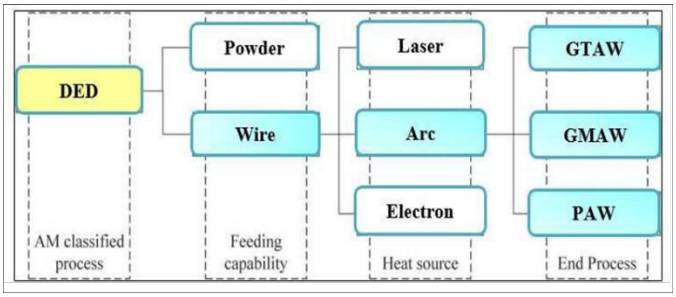

Fig. 1. Typical classification of WAAM [1].

A consumable wire electrode and the workpiece metal generate an electric arc in the GMAW process, where the wire is typically perpendicular to the substrate. Because of its high deposition rate and low heat input, a modified GMAW variation based on a controlled dip transfer mode mechanism has been widely adopted for AM procedures [4,5]. The weld in GTAW and PAW is made with a non-consumable tungsten electrode. In contrast to GMAW, the wire feed angle in GTAW and PAW is changeable and influences the deposit quality, making process planning more difficult [3]. GMAW-based WAAM has a 2-3 times higher deposition rate than GTAW- or PAW-based techniques. Due to the electric current working directly on the feedstock, the GMAW-based WAAM is less stable and produces more weld smoke and spatter. The processing conditions and production rate for a target component are directly influenced by the WAAM technology [6].

2 Experimental

Experiments were carried out using a semi-automated MIG welding system shown schematically in (Figure 2) to build the samples. Lincoln Electric Power MIG (350MP) machine was utilized as a source of energy. The target was building three layers on the substrate with dimensions of (7×70×100) mm using ER70S-6 filler wire with a diameter of 1 mm as a feedstock material, and pure CO_2 as a shielding gas. A low alloy steel plate with dimensions of (9×70×100) mm was used as a substrate for building, as shown in (Figure3(. The oxide layer on the surface of the substrate plate was removed by the use of a wire brush. The WAAM process was however carried out using the parameters shown in (Table 1).

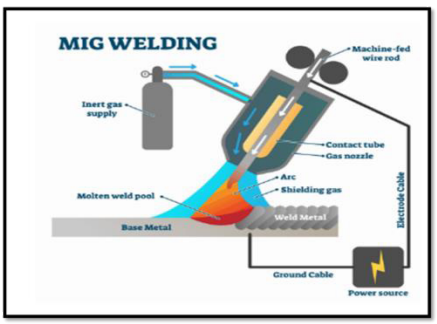

Fig. 2. Schematic representation of the semi-automated MIG welding.

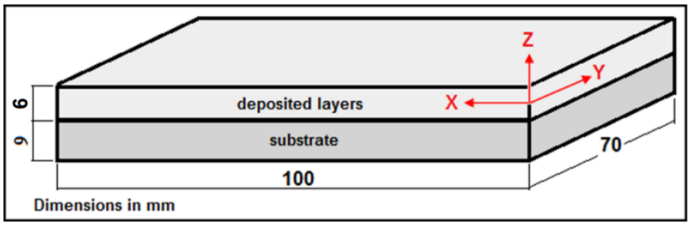

Fig. 3. Deposited layers on the substrate.

Table 1. MIG parameters used with the WAAM process.

Welding current	130 A
Welding Voltage	21V
Wire feeding rate	5 m/min
Travel speed	120 mm/min
Shielding gas	pure CO_2
Gas flow rate	10 l/min
Bead type	Weaving bead
Bead width	8 mm

Five different deposition patterns shown schematically in (Figure 4). The first pattern was longitudinal, in a direction parallel to the X-axis of the substrate (Figure 5), the second pattern was transverse, in a direction parallel to the Y-axis, and the third pattern was a right network of sequentially longitudinal and transverse lines. The fourth deposition pattern was an oblique at an angle of 45°, while the last pattern was an oblique network at an angle of 45° as well. (Table 2) explains the experiments of the current study.

Table 2. Experiments of the current study.

Deposition Pattern	WAAM
Longitudinal	A1
Transverse	A2
Right Network	A3
Oblique	A4
Oblique Network	A5

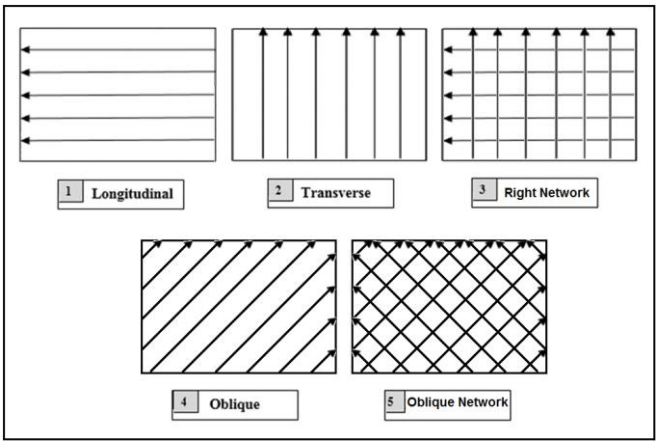

Fig. 4. Deposition patterns of the WAAM.

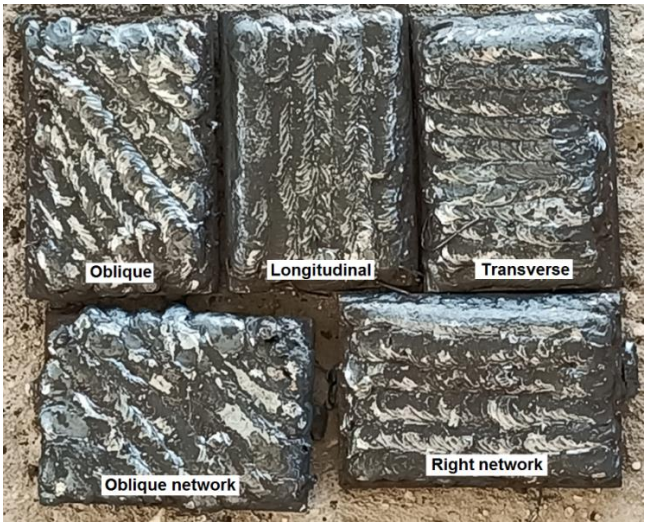

Fig. 5. WAAM samples with five different deposition patterns.

3 Preparation of Test Specimens

Specimens were prepared for tensile, micro-hardness and microscopy (optical and SEM) tests, according to ASTM. The specimens used for the hardness and microscopy tests were cut without removing the substrate material to perform these tests across the interface between the additive layer and the substrate, using BS-712N metal cutting saw machine. For the tensile test specimens, the substrate material was removed using the milling process before extracting the required specimens from the locations shown in (Figure 6).

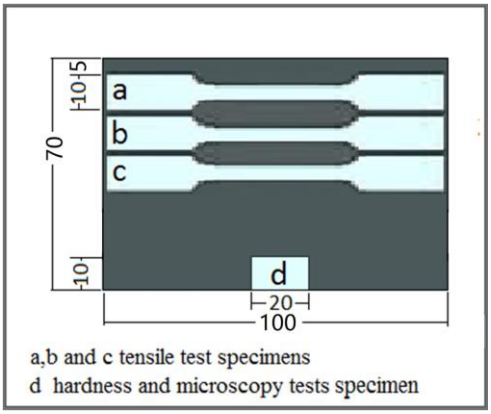

Fig. 6. Locations and dimensions of the test specimens.

3.1 Microscopy

Specimens for microstructural analysis were prepared according to the standard metallographic techniques that involve the following steps.

1. Specimens were cut to a suitable size to facilitate handling and detect the microstructural variations in different zones.

2. The wet grinding process was carried out by exposing the specimen surface to the rotary disk using emery papers of SiC with different grades in sequence (80,220,400, 600, 800, 1000, 1200 and 1500). The specimen was then washed with water and dried with hot air.
3. Mech-anical Polishing; Diamond particles pastes were used to removeing new fine scratche introduced by grinding steps. Polishing was achieve using (3, 1 0.25 μm) pastes sequentially; Special clothing mounted on electrically powered rotary discs were polished.
4. Etching: Nital (2% HNO_3 , 98% Methanol) was used as an etchant to reveal the phases by its chemical effect on the different phases in various levels. After the etching, alcohol was used to clean the ready-to-examine surface.

An optical microscopy was then used to determine microstructure of the diverse regions of additive metal. This test was conducted in the labs of the Department of the Metallurgical Engineering-Faculty of Materials Engineering -University of Babylon. Microstructural examination and chemical composition analysis were carried out using SEM at Al-Razi Center for Metallurgical Examinations in Tehran-Iran. SEM images were taken for all prepared specimens in order to deeply investigate the microstructure with higher magnifications. The specimens were prepared with suitable grinding papers, polished and then etched by nital solution with the same steps as in the optical microscopy. Three regions of the additive metal (upper, middle and lower regions) were studied.

3.2 Mechanical Tests

3.2.1 Micro-hardness test

Micro-hardness test was carried out using digital Vickers micro-hardness tester type (HVS-1000) according to ASTM E384-17. Three regions of the additive metal (upper, middle and lower regions) and were measured after grinding the surfaces being tested. This test was done with a load of 500 g and loading time of 10-15 seconds. The measurement point distribution was by 1.0 mm intervals across the additive layer-substrate interface, with two measurements per point. This test was done at Al-Razi Center for Metallurgical Examinations in Tehran-Iran.

3.2.2 Tension test

Figure 7 shows the shape and dimensions of the tensile test specimen. The specimens were extracted from the additive material by wire electro discharge machining (W-EDM) cut to be as shown in Figure 8. The tensile strength value was an average of three. The test was carried out via universal device WAW-200 China according to (ATSM E8/E8M−13a) with a speed of 1 mm/min. at the labs of the Metallurgical Engineering Department-Faculty of Materials Engineering-University of Babylon.

G=50, W=6, T=5, L=100, A=32, B=30, C=10, R=6 (mm).

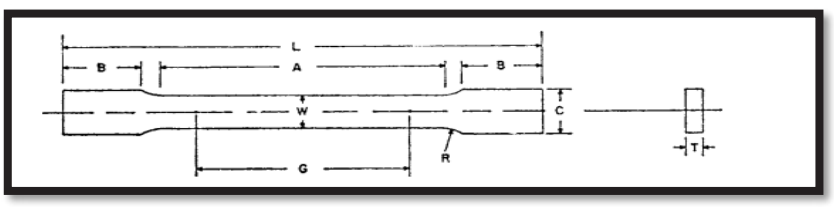

Fig. 7. Shape and dimensions of the tensile test specimen.

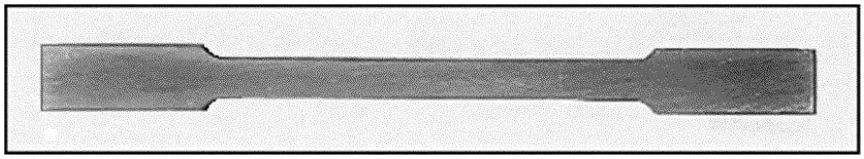

Fig. 8. The prepared tensile test specimen.

4 Results and Discussion

4.1 Microstructure

Microscopy along the cross-section of the additive material deposited longitudinally (A1 in Table 2) shows in (Figure 9) a diversity of microstructure in different regions (upper, middle and lower regions). The dominant structure of the additive material contained, as primary micro-constituents, ferrite and a lower-volume fraction of lamellar pearlite. This is in agreement with that obtained by Ron et al. (2019). The lower region of the additive built material showed a relatively coarse equiaxed grains. It is supposed that the metal grains of the first deposited layers were large columnar as a result of the higher cooling rates to which these layers are exposed due to the rapid absorption of heat by the cold substrate plate. These columnar crystals have been recrystallized to relatively coarse equiaxed grains by the heat of the deposited middle metallic layers. The middle region showed a relatively finer equiaxed grains. It is assumed that the columnar grains of the metal deposited in this region were finer as a result of the lower cooling rates due to the effect of preheating by the previous deposited layers [7]. These columnar grains will then be recrystallized to finer equiaxed grains by the heat of the deposited upper layers. The upper region however exhibited columnar grains because there were no subsequent layers to recrystallize; this is in agreement with that obtained by Aldalur et al. (2020).

The pearlite content in the lower region of the additive built material was more than that in the middle region, which in turn was more than that in the upper region. This is due to the dilution effect with the substrate material [8], which appears more clearly in the built layer/substrate interface region (Figure 10). For the middle and upper regions, the proportion of pearlite was lower, since the carbon content in the filler wire raw material is relatively low (0.08%) [8].

Microstructural examination along the cross-section of the additive material deposited transversely (A2) shows in Figure 11 a diversity of microstructure in different regions. As for the A1, the microstructure of the A2 additive metal consisted of ferrite and pearlite. Shape and size of the grains in the different regions of this sample were similar to that appeared in the A1, except for those of the upper region. The grains in this region were somewhat coarser, and the columnar grains were less compared to those appeared in the upper region of the A1 sample. This could be attributed to the fact that the AM runs required to built layers in A2 sample were more, resulting in accumulation of heat, and thus lower cooling rates [9]. Pearlite distribution was also similar to that in the A1 sample.

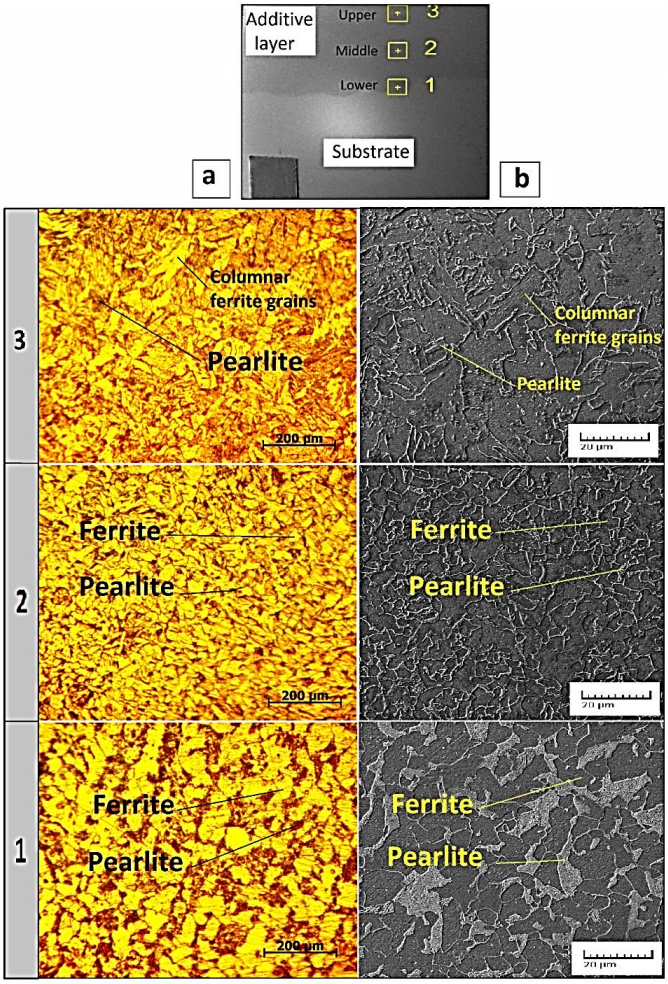

Fig. 9. Micrography of the different regions along the cross-section of the A1 sample using (a): OM and (b): SEM.

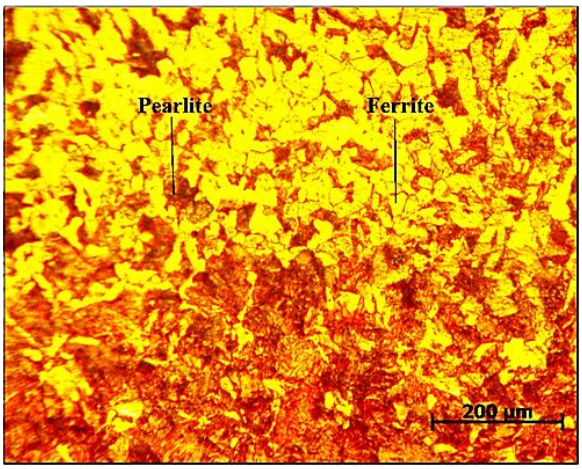

Fig. 10. Microstructure of the built layer/substrate interface region of A1 sample.

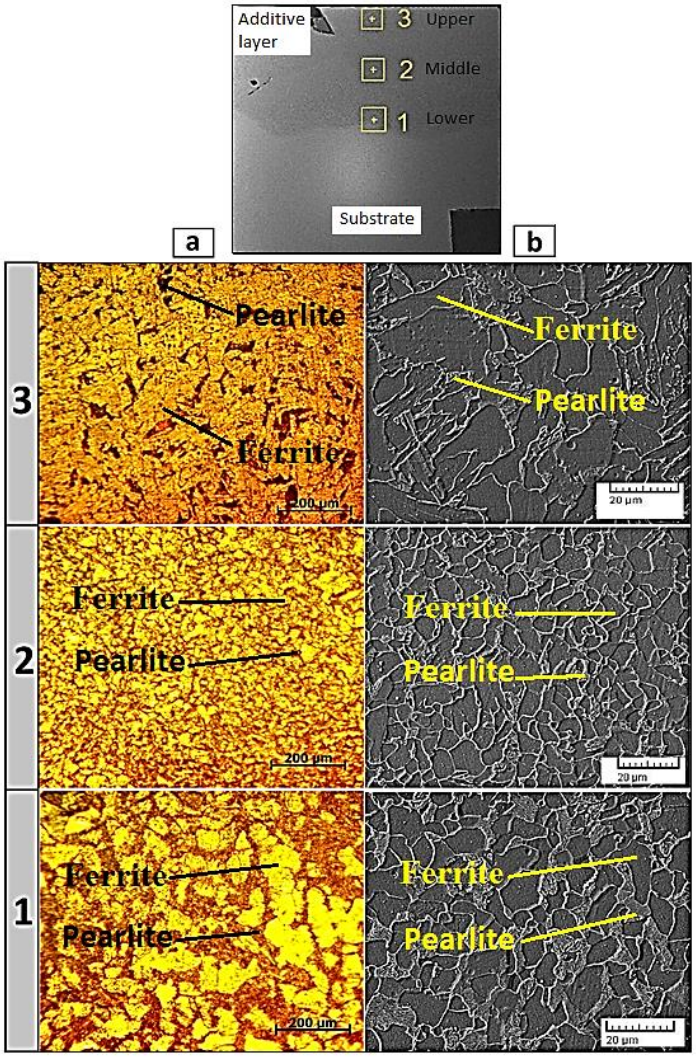

Fig. 11. Micrography of the different regions along the cross-section of the A2 sample using (a): OM and (b): SEM.

For the A3 sample, the microscopy of the lower region showed in Figure 12 a microstructure finer than that appeared in A1 and A2 samples; this is in line with that obtained by Aldalur et al. (2020). This may be due to that the first layer was built longitudinally before depositing the second layer transversely. Therefore, the more runs as a result of the transverse deposition led to the heat accumulation, and thus more recrystallization.

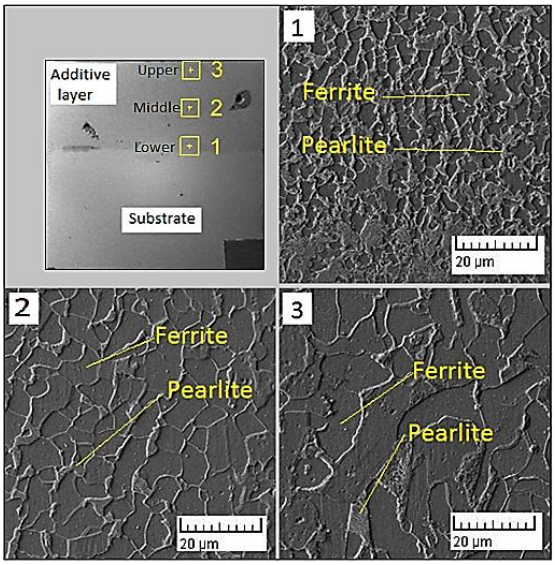

Fig. 12. Microscopy for A3 sample in the different regions using SEM.

Micrography in Figure 13 for the A4 sample showed that the shape and size of the grains in the different regions of this sample were similar to that appeared in the A3, except for those at the lower region. Clearly, the grains in this region were coarser. However, microstructural examination for the A5 sample were similar to that appeared in the A4 as shown in Figure 14.

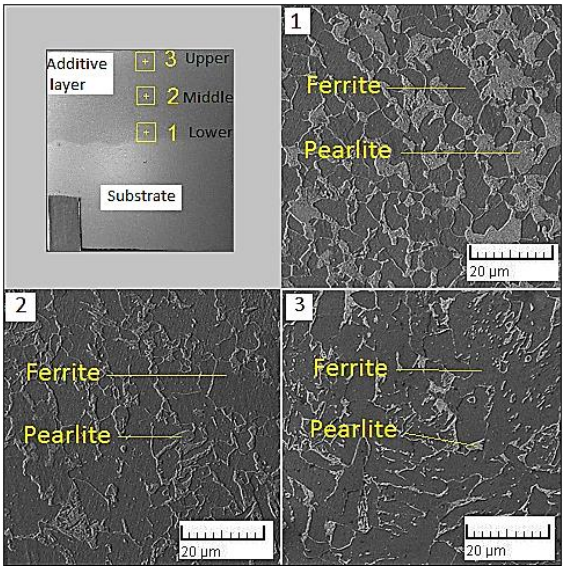

Fig. 13. Micrography for the A4 sample in the different regions using SEM.

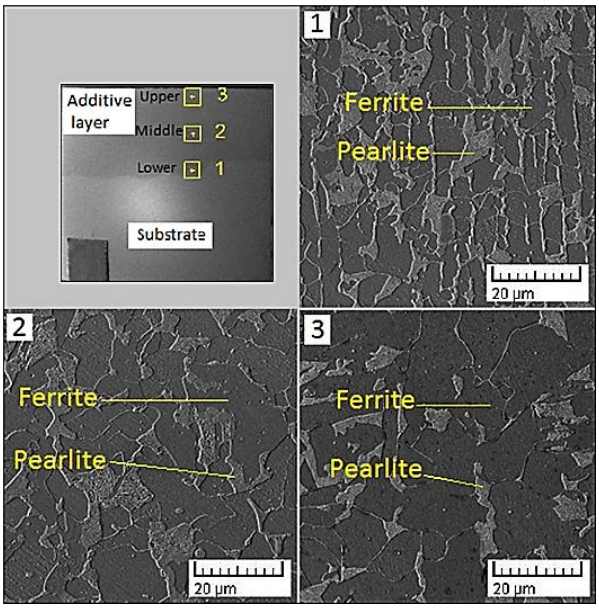

Fig. 14. Microstructure of the A5 sample in the different regions using SEM.

4.2 Hardness

Vickers micro-hardness test along the cross-section of the additive material deposited longitudinally (A1 sample) showed in Figure 15 a diversity of hardness at the different regions (upper, middle and lower regions). Hardness at the lower region was higher, although the equiaxed grains in that region were coarser. This can be attributed to the fact that the fraction of pearlite in that region was higher. The middle region showed less hardness than that at the lower region, because the percentage of pearlite was significantly lower, although the structure of this region was of smaller grain size. The upper region showed less hardness than those at the other regions, for two reasons: the first is that the fraction of pearlite in this region was the lowest, and the second reason is that the particle size in this region was coarser (columnar grains). It is known that the pearlite structure exhibits higher hardness than ferrite due to the presence of the hard cementite phase within the lamellar pearlite structure [10]. It is also known that reducing the particle size leads to an increase in hardness and strength, due to the increase in the amount of grain boundaries, which have higher hardness and strength at room temperature than grains [11]; act as barriers to hinder the dislocations [12].

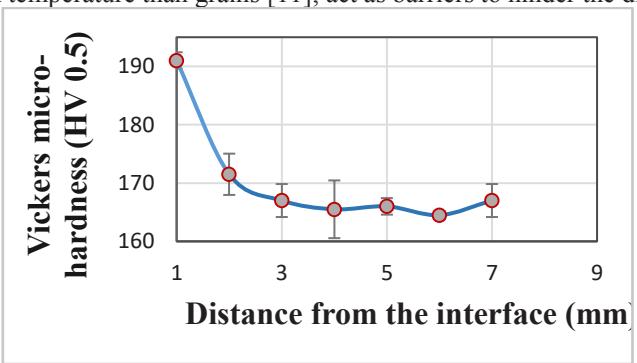

Fig. 15. Hardness distribution across the different regions of A1 sample.

The hardness value at the built layer/substrate interface region was (191HV), which is significantly higher than that of the additive layer material (Figure 15), which in turn is less than that of the substrate material (265HV). This is because the pearlite content in the built layer/substrate interface region was an average between the pearlite content of the substrate and the additive material.

The hardness distribution along the cross-section of the additive material deposited transversely (A2 sample) was similar to that in A1 except for the significant decrease in the hardness values at the upper layers of the sample. This is because the microstructure at that region was somewhat coarse.

The microstructure of the lower region in sample A3 was finer than that in A1 (Figure 12), so the hardness values in that region were somewhat higher, while the rest of the hardness distribution along the cross-section of the A3 sample was similar to A1. Although the structure of the lower region of the sample A4 was coarser than that of A3, hardness at that region was higher. This may be due to the content of pearlite in the region for which the test has been conducted, especially the distribution of pearlite in that region, close to the interface, was not homogeneous.

The hardness distribution along the cross-section of sample A5 was however similar to that of the other samples, with the hardness being highest at the lower region adjacent to the interface, and gradually decreased while advancing towards the upper region. This is due to the effect of the pearlite content as a result of the dilution and the size and shape of the resulting grains. The average Hardness of WAAM samples showed in Figure 16.

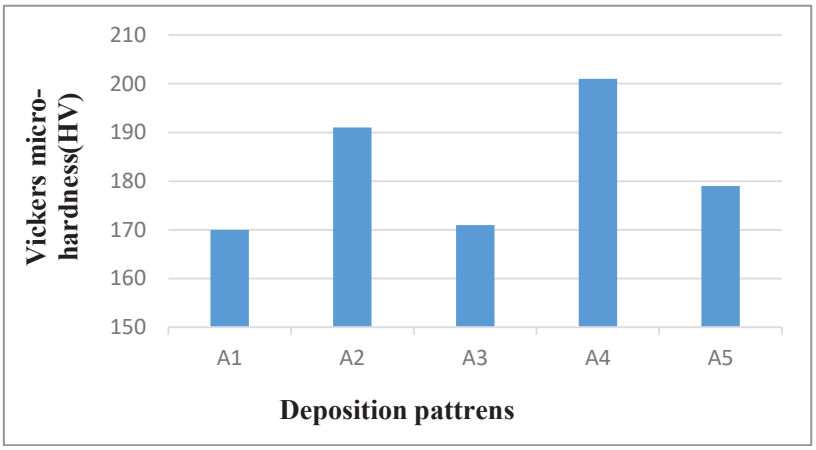

Fig. 16. The average Hardness of WAAM samples.

4.3 Tensione tests

One of the most important goals of this study is to determine the tensile strength of the deposited AM material. Tensile test specimens were extracted from different samples; these specimens include all the deposited layers (upper, middle and lower). The average tensile strength value of the additive material deposited longitudinally (A1 sample) was somewhat high (480 MPa) as shown in Figure 17. This is due to the fact that the direction of tension during the tensile test was parallel to the direction of deposition of the additive layers. The microstructure resulting from the deposition of the metal using this pattern was mostly equiaxed grains with various grain sizes according to the locations of the deposited layers. For the same reason, the fracture was significantly ductile (Figure 18), and the load-deformation curve shown in (Figure 19) proves this, as it is evident from the figure that the elongation was notably large.

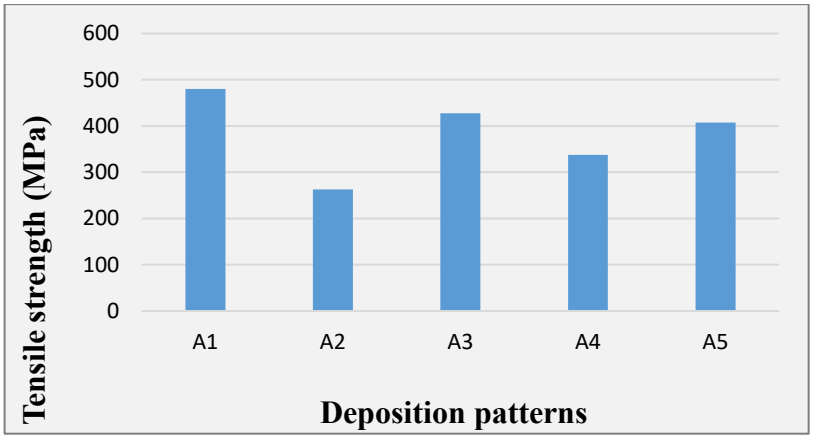

Fig. 17. The average tensile strength of the AM material deposited with the different patterns.

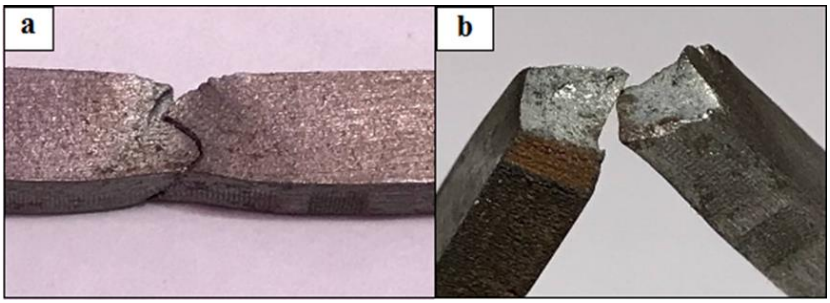

Fig. 18. Fracture of one of the A1 tensile test specimens (a): fracture mode (b): cross-section of fracture.

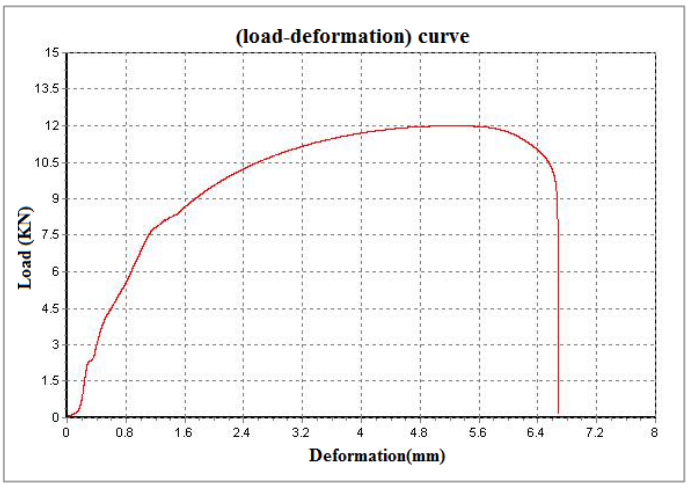

Fig. 19. Load-deformation curve of one of the A1 tensile test specimens.

(Figure 17) shows that the average tensile strength value of the deposited AM material of the A2 sample was (262.5 MPa) significantly lower than that of A1, as it is close to (55%) of the tensile strength of the specimens extracted from the A1 sample. This is consistent with

what was obtained by Waqas et al. (2019). The reason for this relatively low value is that the tension direction was perpendicular to the deposition direction of the additive layers, with a possibility of fracture occurring from convergence regions of the deposition runs for each layer. (Figure 20) shows that the fracture was not ductile as in the A1 sample, but rather brittle. This is also evidenced by the load-deformation curve of this sample, which is shown in Figure 21, where the elongation was much lower.

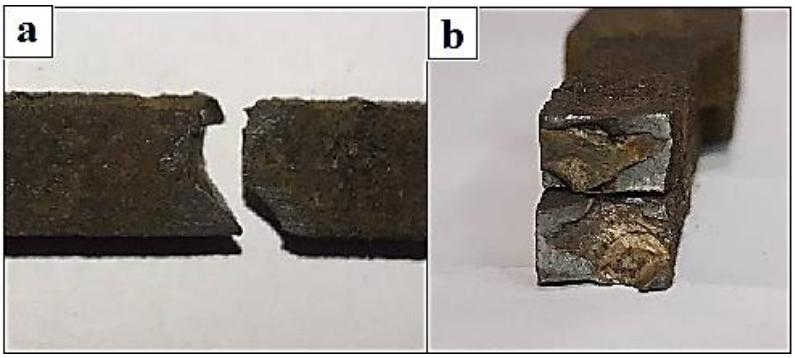

Fig. 20. Fracture of one of the A2 tensile test specimens (a): fracture mode (b): cross-section of fracture.

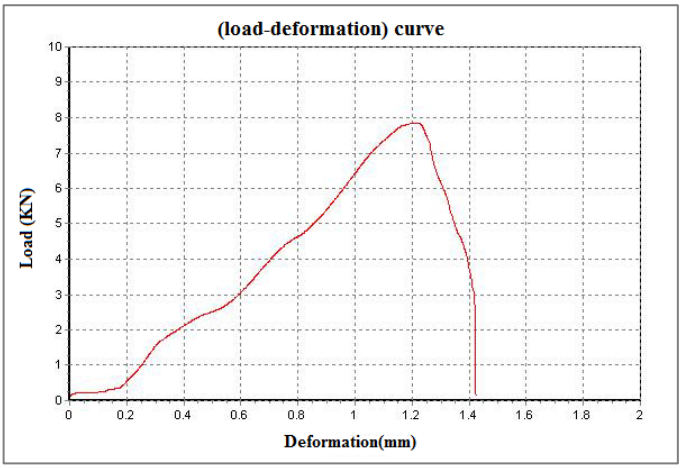

Fig. 21. Load-deformation curve of one of the A2 tensile test specimens.

The average tensile strength value of the specimens extracted from A3 sample was (427.5 MPa), which is about 1.6 times (significantly higher than) that of the A2 sample. This is due to the fact that the deposition of the additive layers was a right network, that is, a network of longitudinal and transverse layers. For the effect of the transversely deposited layers in this pattern, A3 sample had lower tensile strength (about 89%) than that of A1. The fracture was somewhat ductile (Figure 22), and the elongation was higher than that of the A2 sample as in (Figure 23).

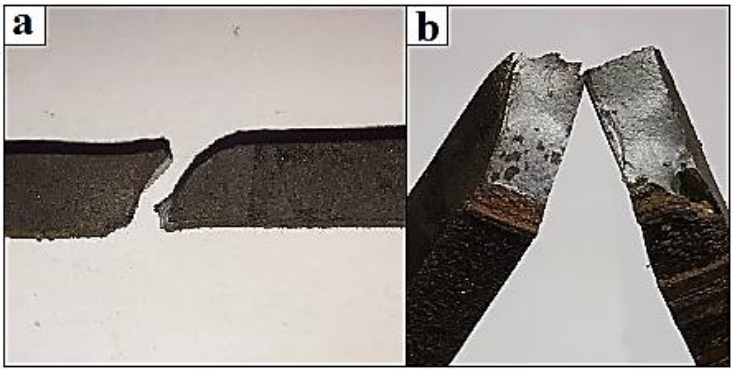

Fig. 22. Fracture of one of the A3 tensile test specimens (a): fracture mode (b): cross-section of fracture.

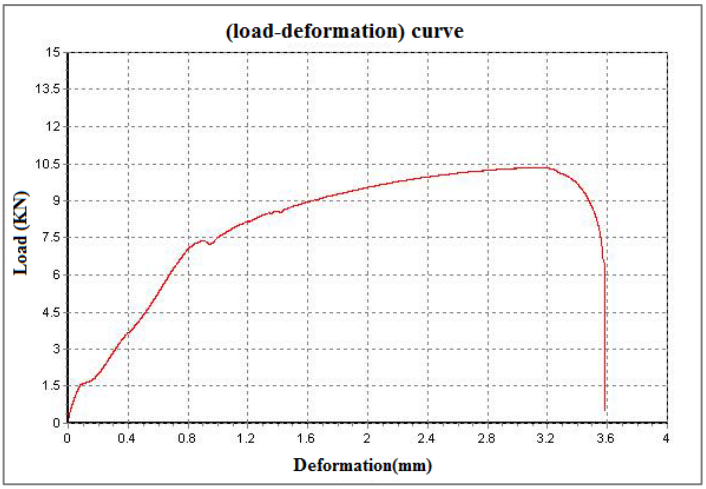

Fig. 23. Load-deformation curve of one of the A3 tensile test specimens.

It is clearly noted from(Figure 17) that the average value of tensile strength for the specimens extracted from A4 sample was (337.5 MPa), which is about an average value between the tensile strength of A1 and A2. This may be due to the analysis of the tensile loading applied during the test into forces parallel to the deposition direction (longitudinal) and perpendicular to the deposition direction (transverse). Figure 24 shows that the fracture was ductile shear at an angle of almost 45° with the direction of the applied load, approximately indicating the deposition angle of the runs of the additive material layers (oblique pattern). This clearly refers to that the fracture occurred along the convergence regions of the deposition runs for each layer. The load-deformation curve shown in Figure 25 indicates that the elongation of A4 sample was notably less than that of A3.

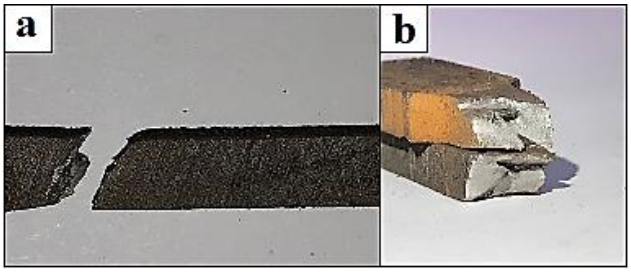

Fig. 24. Fracture of one of the A4 tensile test specimens (a): fracture mode (b): cross-section of fracture.

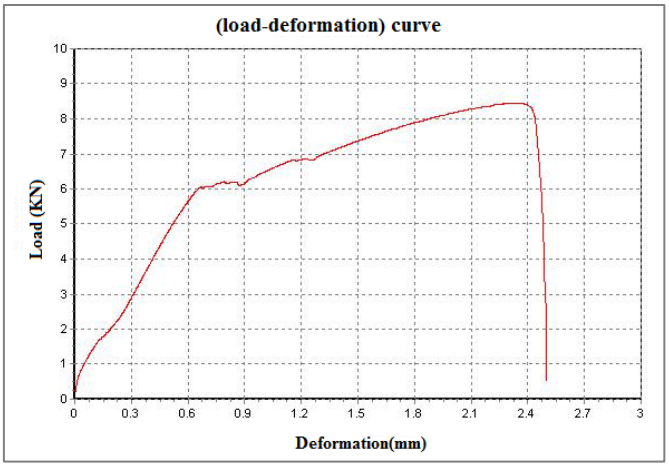

Fig. 25. Load-deformation curve of one of the A4 tensile test specimens.

The average tensile strength value of the specimens extracted from A5 sample was higher than that of A4 (407.5 MPa) as shown in Figure 17. This is definitely a consequence of reducing the shear effect, because the deposition of this pattern was in the form of an oblique network. The fracture was also ductile (Figure 26), and the elongation was remarkably higher, as shown in the load-deformation curve (Figure 27).

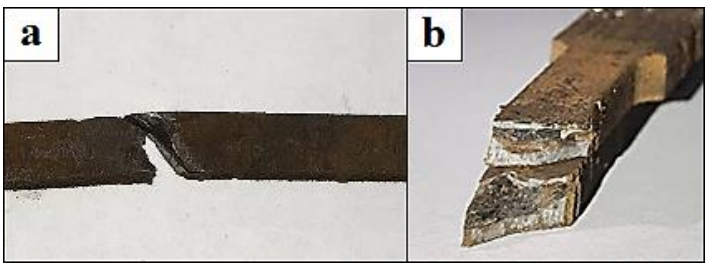

Fig. 26. Fracture of one of the A5 tensile test specimens (a): fracture mode (b): cross-section of fracture.

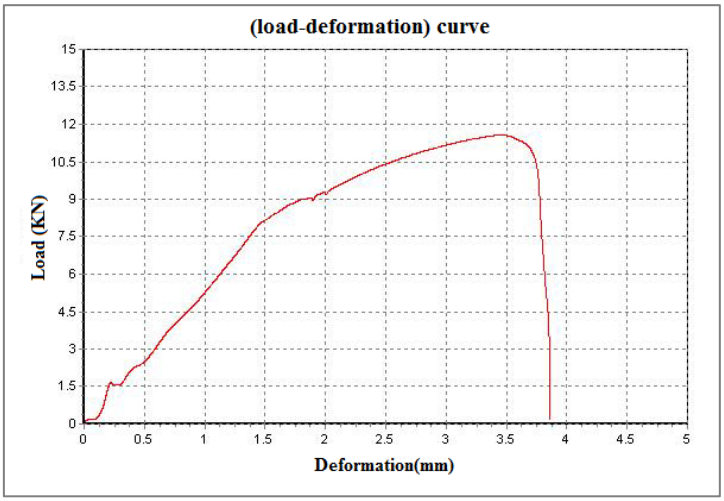

Fig. 27. Load-deformation curve of one of the A5 tensile test specimens.

5 Conclusion

The most significant results of this study can be concluded as follows:

1. The WAAM samples built by different deposition patterns (longitudinal, transverse, right network, oblique and oblique network) showed a diversity of microstructure in different regions. Microscopy generally showed coarse equiaxed grains in the lower regions , fine equiaxed grains in the middle region and columnar grains in the upper regions.
2. The hardness of WAAM samples deposited with the different patterns increased while moving from the upper to the lower regions, where the pearlite content was more as a result of the dilution.
3. The highest average tensile strength value was (480 MPa) for the sample built longitudinally. The fracture mode was significantly ductile. the lowest average tensile strength value was (262.5 MPa) for the sample built transversely, and the fracture mode was brittle.

References

1. K. S. Derekar, Materials science and technology **34(8),** 895-916 (2018)
2. T. A. Rodrigues, et.al, Materials **12(7),** 1121 (2019)
3. D. Ding, Z. Pan, D. Cuiuri, H. Li, The International Journal of Advanced Manufacturing Technology **81(1),** 465-481 (2015)
4. J. Ding, et.al, Computational Materials Science **50(12),** 3315-3322 (2011)
5. P.M. Almeida, S. Williams, *Innovative process model of Ti-6Al-4V additive layer manufacturing using cold metal transfer (CMT),* In 2010 International Solid Freeform Fabrication Symposium. University of Texas at Austin (2010)
6. B. Wu, et.al, Journal of Manufacturing Processes **35,** 127-139 (2018)
7. T. Ron, et.al, Environmental Behavior of Low Carbon Steel Produced by a Wire Arc Additive Manufacturing Process (University of the Negev, Beer-Sheva 8410501, 2019)

8. R. Mehran, et.al, Microstructural evolution and mechanical properties of a low-carbon low-alloy steel produced by wire arc additive manufacturing (Faculty of Engineering and Applied Science, Memorial University of Newfoundland, St. John's, NL A1B 3X5, Canada, 2019).
9. T. L. Van, P. Henri, On the use of gas-metal-arc-welding additive manufacturing for repurposing of low-carbon steel components: microstructures and mechanical properties. Institute of Research and Development (Duy Tan University, Da Nang 550000, Vietnam, 2020)
10. A. R. Tiago, et.al, In-situ strengthening of a high strength low alloy steel during Wire and Arc Additive Manufacturing (WAAM) (Department of Mechanical and Industrial Engineering, NOVA School of Science and Technology, Universidade NOVA de Lisboa, 2829-516 Caparica, Portugal, 2020)
11. M. M. El-Rayes, E. A. El-Danaf, Aluminum Alloy 6082 **212(5),** 1157 – 1168 (2012)
12. B. Bagheri, M. Abbasi, A. Abdollahzadeh, Effect of second-phase particle size and presence of vibration on AZ91/SiC surface composite layer produced by FSP (2020)